Otology & Neurotology
35:e84–e89 © 2014, Otology & Neurotology, Inc.

In Vivo Imaging of Mouse Cochlea by Optical Coherence Tomography

*Yosuke Tona, *Tatsunori Sakamoto, *Takayuki Nakagawa, †Tsunemichi Adachi, *Mirei Taniguchi, *Hiroko Torii, ‡Kiyomi Hamaguchi, *Shin-ichiro Kitajiri, and *Juichi Ito

**Department of Otolaryngology, Head and Neck Surgery, Graduate School of Medicine, Kyoto University, Kyoto; †Adachi ENT Clinic, Kobe; and ‡Department of Otolaryngology, Tenri Hospital, Tenri, Japan*

Hypothesis: Cochlear pathology can be evaluated in living animals using optical coherence tomography (OCT).
Background: The current imaging methods available for the detailed analysis of cochlear pathology in a clinical setting provide only limited information. Thus, a cochlear imaging modality with high definition is needed for improving the diagnosis of cochlear pathology. OCT has been used in other fields for obtaining high-resolution subsurface images, and its use could potentially be extended to the analysis of cochlear pathogenesis.
Methods: *Slc26a4*$^{(-/-)}$ mice, which generate endolymphatic hydrops, and their littermates were used in this study. Auditory function was monitored by the auditory brainstem responses (ABR). After the mice were placed under general anesthesia, OCT images of the cochlea were captured. The cochlea was subsequently dissected out and histologically evaluated. Three or 7 days later, the wild-type mice cochleae were visualized again.
Results: In ABR assessments, *Slc26a4*$^{(-/-)}$ mice showed severe hearing loss, while no significant hearing loss was found in *Slc26a4*$^{(+/-)}$ or *Slc26a4*$^{(+/+)}$ mice. OCT demonstrated normal morphology in the cochlea of both *Slc26a4*$^{(+/-)}$ and *Slc26a4*$^{(+/+)}$ mice, including the location of Reissner's membrane. Meanwhile, in *Slc26a4*$^{(-/-)}$ mice, obvious dislocation of Reissner's membrane was observed, indicating severe endolymphatic hydrops. These findings in the OCT images were consistent with the histologic results for the cochlear morphology, as observed with hematoxylin and eosin staining. Three or 7 days later, wild-type cochleae were successfully visualized using OCT, and no otitis media or labyrinthitis was observed.
Conclusion: OCT can be applied in the detection of endolymphatic hydrops in living mice, indicating the potential of OCT for cochlear imaging analyses for clinical use in the near future.
Key Words: Endolymphatic hydrops—In vivo imaging—Optical coherence tomography—Slc26a4.
Otol Neurotol **35:**e84–e89, 2014.

The development of novel cochlear imaging modalities for improving the detailed analysis of cochlear pathology is an urgent issue because these new imaging modalities will be crucial for the development of new therapeutic options for inner ear diseases. At present, only limited information on intracochlear structures can be obtained clinically. For instance, magnetic resonance images (MRIs) after intratympanic or systemic application of gadolinium-based contrasting agents have been used to detect endolymphatic hydrops in patients who are suspected of having Ménière's disease (1–3). However, the image resolution of MRI is limited in visualizing the details of cochlear pathogenesis. Thin-sheet laser imaging microscopy and related microscopic techniques provide high-resolution images of tissues, including cochlea, without sectioning (4,5). However, this technique requires tissue to be transparent and fluorescent, and thus, its application in rodents and other larger animals, including humans, is difficult.

Optical coherence tomography (OCT) is a noninvasive technique for obtaining subsurface images of opaque materials at a high spatial resolution of 1 to 15 μm (6). The basis of OCT is the use of infrared light to penetrate into the scattering medium (7). This approach is analogous to

Address correspondence and reprint requests to Tatsunori Sakamoto, M.D., Ph.D., Department of Otolaryngology, Head and Neck Surgery, Graduate School of Medicine, Kyoto University 54, Shogoin Kawahara-cho, Sakyo-ku, Kyoto, Japan, 606-8507; E-mail: sakamoto@ent.kuhp.kyoto-u.ac.jp

Conflicts of Interest and Sources of Funding: This work was partly supported by the Innovative Techno-Hub for Integrated Medical Bioimaging of the Project for Developing Innovation Systems, from the Ministry of Education, Culture, Sports, Science and Technology (MEXT), Japan; the Hospital-Company collaboration support project for developing/improving problem-solving-type medical equipment from the Ministry of Economy, Trade and Industry (METI), Japan; and the Promotion Grant for Translational Research at Kyoto University Hospital (FY2010). The authors declare no conflicts of interest.

that of ultrasound B-mode imaging, with the exception that OCT uses light instead of sound. OCT has been clinically applied in the field of ophthalmology for the imaging of the retina and cornea (8,9), as well as in dermatology (10,11). The clinical use of this imaging method has also been extended to the field of cardiology for intravascular imaging of the coronary vessels (12). OCT imaging of the inner ear of normal extracted cochlea (13) and the inner ear structure of living rodents has been reported (14,15). OCT was also used to visualize the pathologic morphology of the tectorial membrane in the isolated cochlea of transgenic Tecta mice, with the apical bony wall removed (16).

The aim of this study was to examine the potential of OCT for the analysis of cochlear pathogenesis in living animals with the bony capsule intact. *Slc26a4* knockout mice are well known as a model for Pendred syndrome (17). In this study, we tested the efficacy of OCT for the visualization of endolymphatic hydrops in living *Slc26a4*$^{(-/-)}$ mice.

MATERIALS AND METHODS

Animals

Mice with targeted disruption of *Slc26a4* (17) and their littermates (*Slc26a4*$^{(-/-)}$, *Slc26a4*$^{(+/-)}$, and *Slc26a4*$^{(+/+)}$) at the age of 11 weeks after birth were used in this study. Animals were maintained at the Institute of Laboratory Animals, Kyoto University, Japan. The Animal Research Committee of the Graduate School of Medicine, Kyoto University, approved all experimental protocols, which were performed in accordance with the National Institute of Health Guidelines for the Care and Use of Laboratory Animals (Approval numbers: MedKyo11516 and MedKyo12172. Primary investigator: TS).

Auditory Function

Auditory brainstem responses (ABRs) were recorded to assess the auditory functions of the experimental animals, as previously described (18). The PowerLab/4sp data acquisition system (AD Instruments, Castle Hiss, Australia) was used for the generation of acoustic stimuli and subsequent recording of the evoked potentials. After the mice had been placed under general anesthesia, subdermal stainless steel needle electrodes were inserted at the vertex (ground), ventrolateral to the measured ear (active), and contralateral to the measuring ear (reference). The acoustic stimuli, consisting of tone burst stimuli (cos^2 rise/fall with a 0.1-ms gate time and a 10-ms plateau) were delivered monoaurally through a speaker (ES1spc; Bioresearch Center, Nagoya, Japan) with a funnel that was fitted into the external auditory meatus. The responses between the ground and the active electrodes were amplified with a digital amplifier (MA2, Tucker-Davis Technologies, Alachua, FL, USA). ABR recordings were performed at frequencies of 8, 16, and 32 kHz.

Optical Coherence Tomography

OCT images in living mice (*Slc26a4*$^{(-/-)}$, *Slc26a4*$^{(+/-)}$, and *Slc26a4*$^{(+/+)}$; n = 2 for each class) were obtained using the OCS1300SS OCT system (Thorlabs, New Jersey, USA), which was equipped with a swept-source light source with a central wavelength of 1,300 nm, a spectral bandwidth of 100 nm, and an average output power of 10 mW. The axial scan rate was 16 kHz. The theoretical axial resolution in water is 9 μm. After the mice were placed under general anesthesia with an intraperitoneal injection of medetomidine (0.5 mg/kg), midazolam (13.3 mg/kg), and butorphanol (0.6 mg/kg), the bulla of the left ear was removed to expose the cochlea. Next, the animal was placed on the scanning stage of the OCT system so that the scanning plane (X-Z plane) was parallel to the midmodiolar section (Fig. 1). OCT images were then obtained.

Histologic Assessment

Immediately after the OCT image acquisition, the animals were euthanized with carbon dioxide and then intracardially perfused with 0.01 M phosphate buffered saline (PBS) at pH 7.4, followed by 4% paraformaldehyde (PFA) in 0.01 M PBS at pH 7.4. Next, the temporal bones were excised, perilymphatically perfused with 4% PFA, and immersed in 4% PFA at 4°C for 4 hours. The specimens were then decalcified with 10% ethylenediamine tetraacetic acid for 7 days. The samples were subsequently embedded and frozen in Tissue-Tec OCT compound (Sakura Finetek, Japan), and midmodiolar cryosections were obtained at a thickness of 10 μm. The cryosections were then stained with hematoxylin and eosin (HE) and viewed with an optical microscope (DP70, Olympus, Japan).

For more detailed morphologic comparisons, cochleae from equivalent mice (*Slc26a4*$^{(+/+)}$, *Slc26a4*$^{(+/-)}$, and *Slc26a4*$^{(-/-)}$) were

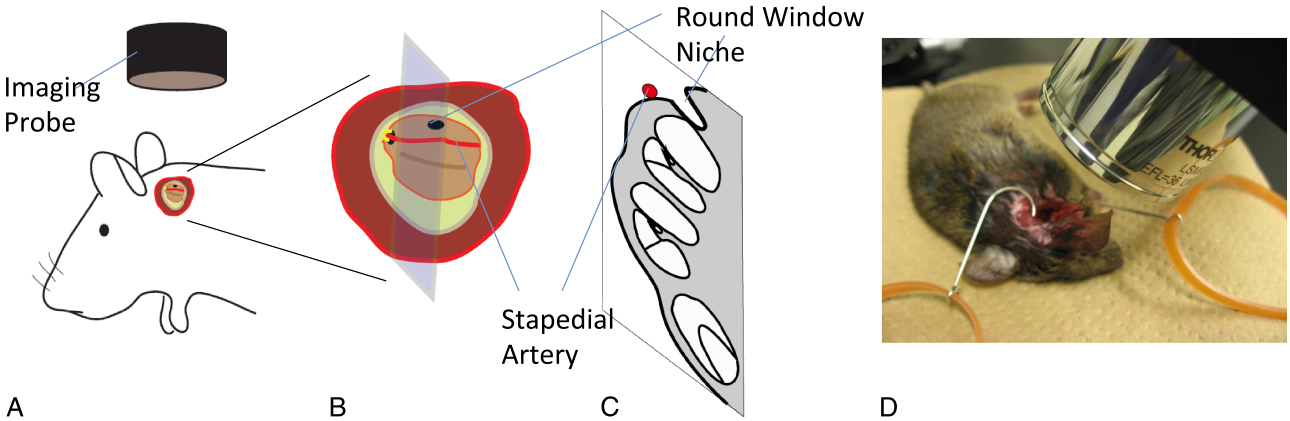

FIG. 1. The scheme of the OCT imaging procedure after surgery. *A*, The mouse was placed under the OCT imaging probe after the exposure of the cochlea. *B*, An enlargement of the surgical field. The optimal section is shown by the rectangle parallel to the modiolus. *C*, The cross section of the intracochlear structures represented by the *rectangle* shown in (*B*). *D*, An overview of the objective lens (outer diameter is 34 mm, working distance is ~25 mm). The animal has been placed on the imaging stage.

isolated, fixed, paraffin-embedded, sectioned at a thickness of 10 μm, stained with HE, and viewed with the optical microscope.

Repeated Observation of the Cochlea Using OCT

For the repeated observation of the cochlea, *Slc26a4*$^{(+/+)}$ mice were used (n = 4). After the first visualization using OCT, the retroauricular skin incision was closed by a nylon monofilament suture, and the animals were maintained in heat-controlled cages. Antibiotic was not administrated. Three or 7 days later, each animal was anesthetized, and OCT images were obtained. The mice were then sacrificed for cryosections as above.

RESULTS

Auditory Functions

The mean left hearing thresholds at the frequencies of 8, 16, and 32 kHz were 10, 15, and 57.5 dB in the *Slc26a4*$^{(+/+)}$ mice and 10, 5, and 30 dB in the *Slc26a4*$^{(+/-)}$ mice,

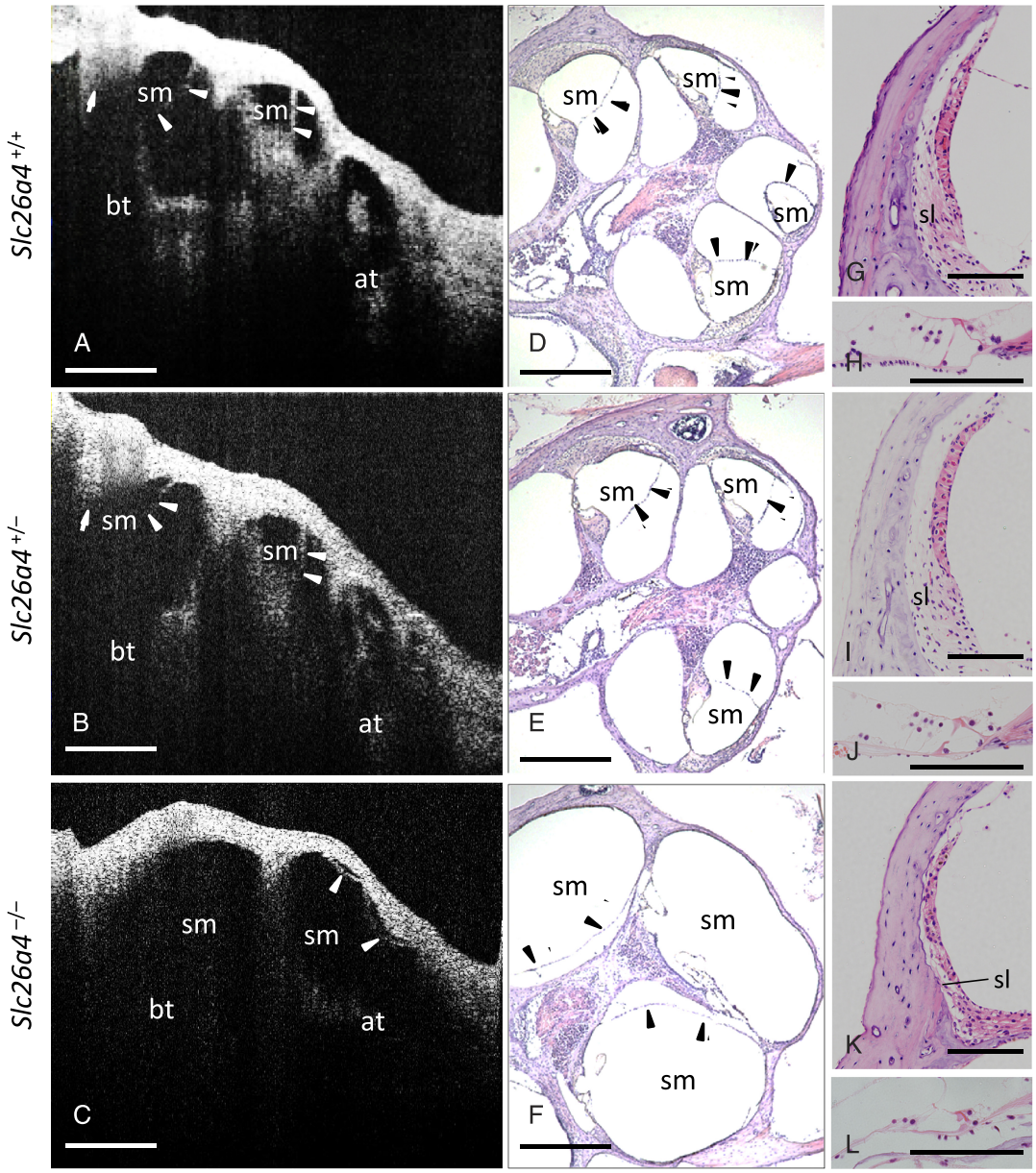

FIG. 2. OCT images and HE staining. *A*, OCT images from a *Slc26a4*$^{(+/+)}$ mouse 11 weeks after birth: apical turn, **at;** basal turn, **bt**; scala media, **sm**. The *arrowheads* indicate the position of Reissner's membrane, and the *arrow* shows the stapedial artery. Reissner's membrane was visualized as a straight, relatively thin structure. *B*, OCT images from a *Slc26a4*$^{(+/-)}$ mouse 11 weeks after birth. The findings were similar to those of a *Slc26a4*$^{(+/+)}$ mouse. *C*, OCT images from a *Slc26a4*$^{(-/-)}$ mouse 11 weeks after birth. Reissner's membrane was positioned close to the bony wall of the scala vestibuli, indicating severe dilatation of the scala media. The cochlea had one and a half turns. *D*, HE staining of the mouse as shown in (*A*). *E*, HE staining of the mouse as shown in (*B*). *F*, HE staining of the mouse as shown in (*C*). (*G, H*), HE staining of a *Slc26a4*$^{(+/+)}$ mouse 11 weeks after birth: spiral ligament, **sl**. (*I* and *J*), HE staining of a *Slc26a4*$^{(+/-)}$ mouse. (*K* and *L*), HE staining of a *Slc26a4*$^{(-/-)}$ mouse. (*A*–*F*), Scale bars = 500 μm, (*G*–*L*), Scale bars = 100 μm.

respectively. In the *Slc26a4*$^{(-/-)}$ mice, no ABR waves were detected at the maximum sound intensities, similar to previous findings (17).

OCT Images

Reissner's membrane in the basal and second turns was clearly demonstrated in the *Slc26a4*$^{(+/+)}$ mice (Fig. 2A) and was visualized as straight lines dividing the scala vestibuli and the scala media. The basilar membrane in the second turn was also depicted. Therefore, the area of the scala media of the second turn was clearly identified by visualization of Reissner's membrane, the lateral bony wall, the basilar membrane, and the cochlear spiral limbus. The cochlear modiolus was detected only at the peripheral end between the apical and second turns. The absorption of light by hemoglobin in the stapedial artery caused the visualization of the area below the vessel to be difficult, concealing the basilar membrane of the basal turn and the vestibule. We therefore chose the second turn for the estimation of endolymphatic hydrops. In the apical turn, the helicotrema was illustrated.

Slc26a4$^{(+/-)}$ mice exhibited similar OCT images to those in *Slc26a4*$^{(+/+)}$ mice (Fig. 2B). The scala media in the second turn showed no dilatation, as demonstrated by straight Reissner's membrane of the second turn, as well by the other surrounding structures, including the basilar membrane, the lateral bony wall, and the cochlear spiral limbus.

The cochlea of *Slc26a4*$^{(-/-)}$ mice had one and a half turns, as previously described (17) (Fig. 2C). In the apical turn, Reissner's membrane was found close to the bony wall of the scala vestibuli, indicating severe dilatation of the scala media. Moreover, the basilar membrane in the apical turn was invisible, suggesting it was appressed to the bony wall of the scala tympani. The size of each turn in the *Slc26a4*$^{(-/-)}$ mice was relatively greater compared with those of *Slc26a4*$^{(+/+)}$ and *Slc26a4*$^{(+/-)}$ mice. The modiolus and the cochlear spiral limbus were not visualized.

HE Staining

In *Slc26a4* $^{(+/+)}$ and *Slc26a4* $^{(+/-)}$ mice, the normal coiling of the 2 and a half turns was confirmed (Fig. 2, D and E). As visualized in the OCT cross sections, Reissner's membrane was found to be straight without convexity, and the scala media was not dilated. The organ of Corti (Fig. 2, H and J), the spiral ligament (Fig. 2, G and H), the spiral ganglions, and the modiolus had no degeneration.

In *Slc26a4* $^{(-/-)}$ mice, the decreased number of turns was histologically confirmed (Fig. 2F). Reissner's membrane showed marked convexity and was close to the bony wall of

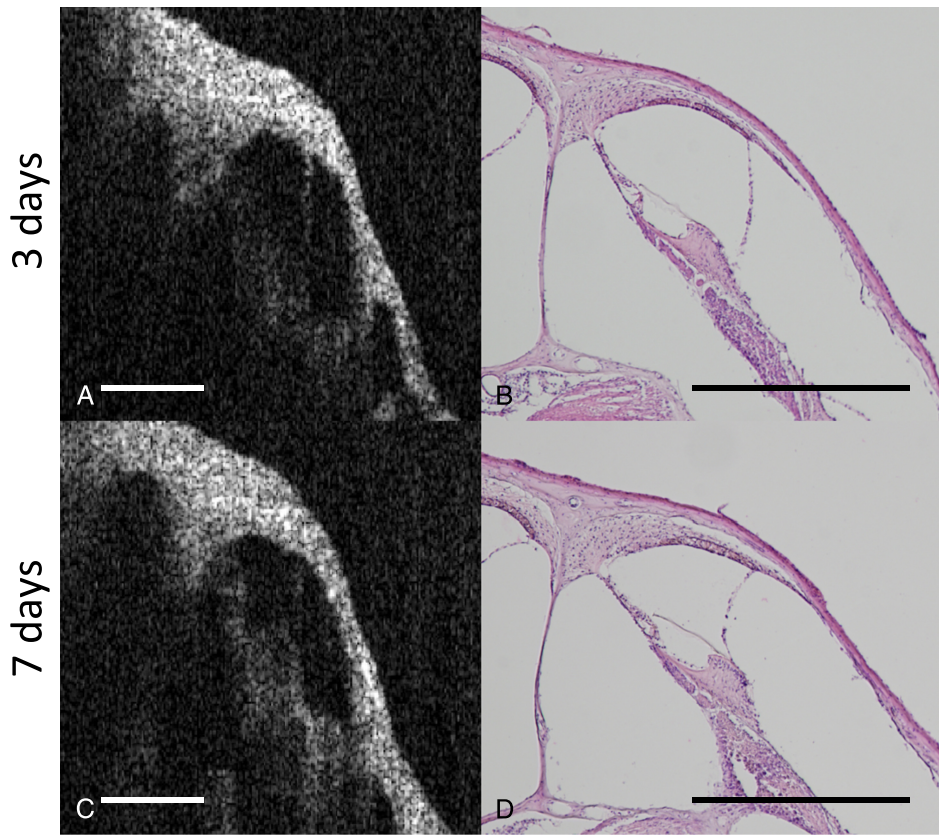

FIG. 3. Repeated visualization of the cochlea by OCT. OCT images of *Slc26a4*$^{(+/+)}$ mice cochlea 3 or 7 days after the first visualization (*A* and *C*, respectively) showed normally positioned Reissner's and basilar membranes. HE staining of the same cochlea (*B* and *D*, respectively) showed no endolymphatic hydrops and no obvious infiltration of inflammatory cells in the middle ear mucosa and inner ear. Scale bars = 500 μm.

the scala vestibuli, as shown in the OCT images. The basilar membrane was adjacent to the bony wall of the scala tympani. The spiral ligament was thinner (Fig. 2K) than that of *Slc26a4*$^{(+/+)}$ and *Slc26a4*$^{(+/-)}$ mice (Fig. 2, G and I), and the outer hair cells in the organ of Corti were degenerated (Fig. 2L). These findings were not observed using OCT (Fig. 2C) and were consistent with those of a previous report (17,19,20).

Repeated Observation of the Cochlea Using OCT

All the mice were alive at 3 or 7 days after the first visualization of the cochlea in *Slc26a4*$^{(+/+)}$ mice using OCT. The mice were anesthetized, and the middle ear was reopened. No obvious infectious pus was present in the middle ear. After the removal of the fibrin clots, OCT images were successfully obtained (Fig. 3, A and C). The intracochlear morphology, including the position of Reissner's and basilar membranes, was normal in all the OCT images. After OCT imaging, each cochlea was removed and processed for histologic assessment. In the HE images, there was no dilatation of the scala media and no obvious inflammatory cell infiltration in the middle ear mucosa and the inner ear (Fig. 3, B and D).

DISCUSSION

In this study, we investigated the potential of OCT for the analysis of cochlear pathogenesis by examining its ability to illustrate the cochlear phenotype of *Slc26a4*$^{(-/-)}$ mice in vivo. The *Slc26a4*$^{(-/-)}$ mice were completely deaf, and the HE specimens revealed a decreased number of cochlear turns, marked convexity of Reissner's membranes, basilar membranes adjacent to the bony wall of the scala tympani, degenerated hair cells, and a thinned spiral ligament, all of which were the same findings as previously reported (17). OCT was able to detect the decreased number of cochlear turns and the extremely distended Reissner's membrane, indicating the marked dilatation of the scala media. Therefore, OCT is considered a useful device for the evaluation of endolymphatic hydrops in living mice. However, OCT had difficulties in showing the basilar membranes, the cochlear modiolus, the spiral limbus, and hair cells in *Slc26a4*$^{(-/-)}$ mice. The basilar membrane was invisible in OCT images of *Slc26a4*$^{(-/-)}$ mice because of the proximity of the basilar membrane to the adjacent bony wall. Meanwhile, the cochlear modiolus and the spiral limbus were too deep for OCT to visualize in *Slc26a4*$^{(-/-)}$ mice because of the limitation of the penetration depth. More detailed axial resolution at a greater depth (additional micrometers) was needed to evaluate the extent of hair cell degeneration.

In this study, the cochlear bony walls of living mice were exposed through the removal of the bulla. Mice are known to survive after the removal of the bulla, even when followed by cell transplantation (21,22). Furthermore, we showed that repeated visualization of the cochlea in living mice 3 or 7 days after the first visualization was possible by this method without inducing endolymphatic hydrops, otitis media, or labyrinthitis. Thus, this strategy can be used, for example, in the evaluation of dynamic changes in the inner ear of living animals that have received a particular drug to induce or reduce endolymphatic hydrops.

MRI and micro-CT are the other imaging modalities capable of visualizing the detailed inner structures inside the cochlea. MRI has been already applied to humans and is able to illustrate much deeper views than OCT. In addition, MRI has the ability to reveal the area of the scala media by enhancing the signal from the perilymph by intratympanic or systemic administration of a contrast agent (1–3). However, MRI is unable to show minute structures such as Reissner's membrane because its axial resolution is about 0.5 to 1.0 mm. Moreover, the use of contrast agents contains the risk of inner ear impairment when administered locally and the possibility of nephrogenic systemic fibrosis when administered systemically (23). Although micro-CT has an axial resolution of about 1 to 100 μm (24), this method is not acceptable for living animals because of the serious tissue damage that results from the high-dose ionizing radiation (25).

The thick cochlear bony capsule in humans is an obstacle to the clinical application of OCT as a cochlear imaging modality; however, we believe that OCT can be applied in humans at least for the visualization of the endolymphatic hydrops in the lower part of the cochlea or the vestibule by visualization through the round window membrane, which is accessible through tympanostomy using a side-viewing OCT fiber (26). OCT is also available for experimental use. A previous report from Kimura and Schuknecht (27) demonstrated that obliteration of the endolymphatic sac in guinea pigs was capable of producing endolymphatic hydrops. Moreover, various procedures to elicit inner ear autoimmune disease have been reported. (28,29) The extent of endolymphatic hydrops in both models were only evaluated in samples obtained after the animals were sacrificed. OCT enables the sequential visualization of endolymphatic hydrops without sacrificing the animals. Therefore, OCT is applicable for the evaluation of various drugs for the treatment of Ménière's disease.

The present findings demonstrate that OCT can be used to evaluate the gross anatomy of mouse cochlea, including the location of Reissner's membrane and the basilar membrane. The use of OCT contributes to the evaluation of pathologic changes in the cochlea of living mice.

Acknowledgments: The authors thank Konrad Noben Trauth, Andrew Griffith, and Eric Green at the National Institute of Health (NIH) and Tsutomu Nakashima at the Department of Otorhinolaryngology, Nagoya University Graduate School of Medicine, for the generous donation of *Slc26a4*-disrupted mice.

REFERENCES

1. Zou J, Poe D, Bjelke B, Pyykkö I. Visualization of inner ear disorders with MRI in vivo: from animal models to human application. *Acta Otolaryngol Suppl* 2009;22–31.
2. Naganawa S, Satake H, Iwano S, Fukatsu H, Sone M, Nakashima T. Imaging endolymphatic hydrops at 3 Tesla using 3D-FLAIR

with intratympanic Gd-DTPA administration. *Magn Reson Med Sci* 2008;7:85–91.
3. Sano R, Teranishi M, Yamazaki M, et al. Contrast enhancement of the inner ear in magnetic resonance images taken at 10 minutes or 4 hours after intravenous gadolinium injection. *Acta Otolaryngol* 2012;132:241–6.
4. Santi PA. Light sheet fluorescence microscopy: a review. *J Histchem Cytochem* 2011;59:129–38.
5. Kopecky BJ, Duncan JS, Slliott KL, Fritzsch B. Three-dimensional reconstructions from optical sections of thick mouse inner ears using confocal microscopy. *J Microsc* 2012;248:292–8.
6. Fujimoto JG, Farkas D. *Biomedical Optical Imaging*. Oxford, UK: Oxford University Press, USA, 2009.
7. Huang D, Swanson EA, Lin CP, et al. Optical coherence tomography. *Science* 1991;254:1178–81.
8. Spaide RF, Koizumi H, Pozonni MC. Enhanced depth imaging spectral-domain optical coherence tomography. *Am J Ophthalmol* 2008;146:496–500.
9. Shah SU, Kaliki S, Shields CL, Ferenczy SR, Harmon SA, Shields JA. Enhanced depth imaging optical coherence tomography of choroidal nevus in 104 cases. *Ophthalmology* 2012;119:1066–72.
10. Collier T, Arifler D, Malpica A, Follen M, Richards-Kortum R. Determination of epithelial tissue scattering coefficient using confocal microscopy. *IEEE J Sel Top Quantum Electron* 2003;9:307–13.
11. Pierce MC, Strasswimmer J, Park BH, Cense B, de Boer JF. Advances in optical coherence tomography imaging for dermatology. *J Investig Dermatol* 2004;123:458–63.
12. Unal G, Carlier SG. In-vivo optical coherence tomography image analysis. *Biomedical Imaging: From Nano to Macro, 2010 IEEE International Symposium on* 2010;1409–10.
13. Wong BJF, Zhao Y, Yamaguchi M, Nassif N, Chen Z, de Boer JF. Imaging the internal structure of the rat cochlea using optical coherence tomography at 0.827 microm and 1.3 microm. *Otolaryngol Head Neck Surg* 2004;130:334–8.
14. Lin J, Staecker H, Jafri MS. Optical coherence tomography imaging of the inner ear: a feasibility study with implications for cochlear implantation. *Ann Otol Rhinol Laryngol* 2008;117:341–6.
15. Subhash HM, Davila V, Sun H, Nguyen-Huynh AT, Nuttall AL, Wang RK. Volumetric in vivo imaging of intracochlear microstructures in mice by high-speed spectral domain optical coherence tomography. *J Biomed Opt* 2010;15:036024.
16. Gao SS, Xia A, Yuan T, et al. Quantitative imaging of cochlear soft tissues in wild-type and hearing-impaired transgenic mice by spectral domain optical coherence tomography. *Opt Express* 2011;19:15415–28.
17. Everett LA, Belyantseva IA, Noben-Trauth K, et al. Targeted disruption of mouse Pds provides insight about the inner-ear defects encountered in Pendred syndrome. *Hum Mol Genet* 2001;10:153–61.
18. Kada S, Nakagawa T, Ito J. A mouse model for degeneration of the spiral ligament. *J Assoc Res Otolaryngol* 2009;10:161–72.
19. Everett LA, Glaser B, Beck JC, et al. Pendred syndrome is caused by mutations in a putative sulphate transporter gene (PDS). Nat Genet. *Nature Publishing Group* 1997;17:411–22.
20. Wangemann P, Itza EM, Albrecht B, et al. Loss of KCNJ10 protein expression abolishes endocochlear potential and causes deafness in Pendred syndrome mouse model. *BMC Med* 2004;2:30.
21. Sharif S, Nakagawa T, Ohno T, et al. The potential use of bone marrow stromal cells for cochlear cell therapy. *Neuroreport* 2007;18:351–4.
22. Nishimura K, Nakagawa T, Sakamoto T, Ito J. Fates of murine pluripotent stem cell-derived neural progenitors following transplantation into mouse cochleae. *Cell Transplant* 2012;21:763–71.
23. Goenka AHA, Das CJC, Sharma RR. Nephrogenic systemic fibrosis: a review of the new conundrum. *Natl Med J India* 2009;22:302–6.
24. Li XX, Anton NN, Zuber GG, et al. Iodinated α-tocopherol nanoemulsions as non-toxic contrast agents for preclinical X-ray imaging. *Biomaterials* 2012;34:481–91.
25. Saito S, Murase K. Detection and early phase assessment of radiation-induced lung injury in mice using micro-CT. *PLoS ONE* 2012;7:e45960.
26. Wu Y, Xi J, Huo L, et al. Robust high-resolution fine OCT needle for side-viewing interstitial tissue imaging. *IEEE J Sel Top Quantum Electron* 2010;16:863–9.
27. Kimura RS, Schuknecht HF. Membranous hydrops in the inner ear of the guinea pig after obliteration of the endolymphatic sac. *Pract Otorhinolaryngol (Basel)* 1965;27:343–54.
28. Gates GAG. Ménière's disease review 2005. *J Am Acad Audiol* 2005;17:16–26.
29. Tomiyama SS. Development of endolymphatic hydrops following immune response in the endolymphatic sac of the guinea pig. *Acta Otolaryngol* 1991;112:470–8.